Chemical Engineering Journal 502 (2024) 158001

Contents lists available at ScienceDirect

Chemical Engineering Journal

journal homepage: www.elsevier.com/locate/cej

Excellent cycle stability of Fe loaded on N-doped activated carbon for microwave hydrogenolysis of lignin

Junhao Cui [a], Zhiyang Zhao [a], Yongqi Ren [a], Bailong Chen [a], Chase Rheinlander [b], Antonio Xavier Moore [c], Longzhi Li [a,*]

[a] College of Mechanical and Electronic Engineering, Shandong University of Science and Technology, 266590 Qingdao, Shandong Province, China
[b] Department of Chemistry and Physics, College of Science, The University of Texas Permian Basin, 79762 Odessa, TX, United States
[c] Department of Life and Physical Sciences, Fisk University, 37208 Nashville, TN, United States

ARTICLE INFO

Keywords:
Microwave-assisted hydrogenolysis
Lignin
Fe/N-AC
Cycle stability

ABSTRACT

Microwave-assisted hydrogenolysis of lignin is an emerging alternative to conventional depolymerization capable of converting lignin into aromatic compounds. Activated carbon (AC) supported Fe component have been shown to be cost-effective for this process, but its cycle stability needs to be improved due to Fe agglomeration. Herein, a strategy of nitrogen doping to promote stability was developed, which utilized melamine ($C_3H_6N_6$) as nitrogen source to prepare the catalyst of N-doped AC supported Fe (Fe/N-AC). The catalyst characterization indicated that the N-doped AC acted as anchor points for Fe components, avoiding catalyst deactivation from the source. Fe/N-AC presented an excellent cycle stability, remaining a phenolic compound selectivity of 93.3 % after five cycles and a decrease of only 4.79 % (compared to the first). The DFT calculation results revealed that Fe/N-AC tended to break C_{Ar}-OCH_3 during the hydrogenolysis of guaiacol, with an energy barrier of 0.877 eV. This work proposes a simple and effective strategy to improve the stability of lignin hydrogenolysis catalysts, providing important references for the high-valued utilization of lignin.

1. Introduction

Lignocellulose is an important source of biomass energy and considered to be one of the most promising feedstocks for sustainable chemical and fuel production [1]. Lignocellulose is composed of three main components, namely, lignin, cellulose, and hemicellulose [2]. Second to cellulose, lignin is currently the most abundant natural polymer that consists of different phenylpropane [3]. The complex structure of lignin gives it high steric hindrance, resulting in low reactivity [4]. Therefore, the efficient conversion of lignin into aromatic compounds such as phenol remains a great challenge. Lignin is connected by different C-O (contributes to 40 %-70 %) and C-C bonds, including α-O-4, β-O-4, 4-O-5, β-β and β-5 bonds [5,6]. Breaking the C-C bonds can directly decompose lignin into short carbon chains, which helps to produce small molecule hydrocarbons as fuels. However, the bond dissociation energy (BDE) of C-C bonds reaches 334–502 kJ·mol^{-1}, making bonds breaking inefficient and energy consuming. The breaking of C-O bonds mainly produces phenolic, aldehyde and ester compounds containing aromatic rings. In contrast, the BDE of α-O-4 and β-O-4 are 215–240 kJ·mol^{-1} and 290–315 kJ·mol^{-1}, respectively, which are lower than that of C-C bonds [7–9]. Thus, selective breakage of C-O bonds is the better alternative for producing aromatic compounds.

Depolymerization is an effective way to achieve selective breakage of C-O bonds. Depolymerization of lignin involves enzymatic depolymerization, oxidative depolymerization and thermal depolymerization [3]. The challenge of enzymatic depolymerization is the method has stringent requirements for temperature and pH, making industrial application difficult [10]. The reaction temperature for oxidative depolymerization is usually low (0–250 °C), however, it tends to cause the opening of the benzene ring and usually be carried out under alkaline conditions to result in the equipment corrosion [11]. The bio-oil yield from conventional thermal depolymerization is typically limited due to the undesirable characteristics including low pH, high viscosity, high oxygen content and poor stability [12,13]. Hydrogenolysis, that is the breaking of bonds with simultaneous hydrodeoxygenation of lignin intermediates, is of interest because of its ability to efficiently convert lignin to aromatic compounds [14–16]. Hydrogen-donors are classified into external hydrogen-donor and in-situ hydrogen-donor. External

* Corresponding author.
E-mail address: lilongzhi630@163.com (L. Li).

https://doi.org/10.1016/j.cej.2024.158001
Received 26 July 2024; Received in revised form 25 October 2024; Accepted 23 November 2024
Available online 24 November 2024

hydrogen-donors can add to both the cost and danger of the process, and are prone to over-hydrogenate the benzene ring [17,18]. In contrast, the use of hydrogen-donor solvents is potentially safer and more cost-effective. The well-known hydrogen-donor solvents consist of FA, AcOH, MeOH, EtOH, i-PrOH and BuOH. For this method, the highly active hydrogen radicals can inhibit the recombination of intermediates, thus reducing the coking rate and improving the selectivity of target products.

Microwaves are electromagnetic waves with frequencies ranging from 300 MHz to 300 GHz. The commonly used microwave frequencies in industry and laboratories are 915 MHz and 2450 MHz. Microwave heating is a method by molecular friction and dielectric loss of dipoles or ions in the material, realizing the more uniform heating and direct heating of material. Besides, microwave heating can form a temperature gradient from inside to outside, different from traditional heating. As a result, the utilization of microwave heating for lignin conversion can also reduce heat loss, but also quickly heat lignin to the desired temperature, effectively improving the yield and quality of bio-oil [19]. Microwave-assisted hydrogenolysis of lignin can induce the activation of C-O bonds by hydrogen radicals under electromagnetic fields, thereby increasing the selectivity of target product [20]. It was recently found that microwave-assisted hydrogenolysis of lignin in the mixture of water-alcohol over commercial catalysts (Pd/C, Pt/C, Ru/C) obtained 65 wt% yield of phenolic monomers [21]. The design of highly active and selective catalysts is crucial for microwave-assisted hydrogenolysis of lignin. Fe exhibits excellent reactivity in lignin hydrogenolysis and activates C-O bonds to a certain extent. Moreover, Fe is advantageous due to its high cost-effectiveness and easy availability. However, Fe exhibits poor catalytic stability, mainly due to the aggregation of Fe components. Considering this, ensuring the dispersion of Fe components during catalyst preparation is crucial, requiring enhanced interactions between Fe and support. At present, AC supported Fe catalysts are widely used in microwave-assisted hydrogenolysis of lignin. AC possesses excellent microwave absorption properties and well-developed pores. However, the interaction between AC and Fe components is relatively weak, creating a challenge of catalyst aggregation and deactivation that leads to low efficiency in lignin hydrogenolysis [22]. Nitrogen doping provides a stable coordination environment for AC so that the metal components can be better anchored in the AC [23]. It is reported that N-doped carbon catalysts can exhibit excellent metal-support effect and enable an effective control of Fe oxidation state via an electronic interaction between Fe and N, which keeps Fe highly stable during the hydrodeoxygenation of m-cresol [24]. Doping nitrogen can also form Fe-N_x coordination bonds, which can anchor metal components, thus promoting the dispersion of Fe [22]. Recent studies have shown that Fe/N-AC has better oxidative depolymerization properties for lignin, and the molecular mass of oxidized lignin was significantly reduced [25]. Currently, there is limited attention on the fundamental impact of nitrogen doping for catalytic stability and its intrinsic role in microwave-assisted lignin hydrogenolysis remains poorly understood.

Herein, Fe/N-AC was prepared by solution impregnation and used for microwave-assisted hydrogenolysis of lignin. The effects of hydrogen-donor solvents on lignin depolymerization were investigated, and the characteristics of hydrogenolysis products were examined. The cyclic utilization of catalysts under microwave-assisted hydrogenolysis was investigated to examine the effect of nitrogen doping on catalyst stability. On the basis, the work paid more attention to search the likely path of microwave-assisted hydrogenolysis of lignin through DFT simulation, for purpose of investigating the effect of nitrogen doping on the mechanism of lignin hydrogenolysis.

2. Experimental and methods

2.1. Materials and reagents

Alkaline lignin that was purchased from Shanghai Macklin Biochemical Co., Ltd and was used for microwave-assisted hydrogenolysis. Before the hydrogenolysis, lignin was crushed and sieved to 100–120 mesh. $Fe(NO_3)_3$ and melamine ($C_3H_6N_6$) was mixed with activated carbon (AC) to develop the catalysts. $Fe(NO_3)_3$ and $C_3H_6N_6$ were provided by Shanghai Macklin Biochemical Co., Ltd. The AC was purchased from Shanghai Aladdin Biochemical Technology Co., Ltd. MeOH, EtOH and i-PrOH were used as hydrogen-donor solvents.

2.2. Catalyst preparation and characterization

AC, $Fe(NO_3)_3$, and $C_3H_6N_6$ were dissolved in 40 mL EtOH according to a certain ratio. Fig. 1**a** displays the main devices used for the catalyst preparation, consisting of ultrasonic cleaner, water bath, drying cabinet, ball mill, and tube furnace. The mixture of AC and melamine firstly underwent ultrasonic oscillation treatment in the ultrasonic cleaner for 1 h, followed by stirring, drying and grinding in the water bath, drying oven and ball mill to obtain the modified AC, respectively. Subsequently, the modified AC was placed in the tube furnace and heated to the setting temperature according to the temperature program (**Fig.S1**). Prior to the heating, the vacuum pump was utilized to completely evacuate the residual air in the tube furnace. During the heating process, nitrogen was continuously imported into the tube furnace at flow rate of 40 mL/min to maintain an inert atmosphere. The prepared catalyst was denoted as Fe/N-AC. $Fe(NO_3)_3$ was loaded into AC at the ratio of 1 mmol/g, and AC was doped with $C_3H_6N_6$ at the mass ratio of 1:9. To verify the activity effect of metal components and the anchoring effect of nitrogen doping, N-AC and Fe/AC are prepared according to a similar procedure to that described above. The N-AC with calcination temperatures of 600 °C and 800 °C were named $N\text{-}AC_{600}$ and $N\text{-}AC_{800}$, respectively.

The crystal structures and species of the catalysts were determined by X-ray diffraction (XRD) analyzer (D8 Advance, Bruker), operated at the 2θ° range from 20 ~ 70° and with a scanning speed of 4°/min. The spectrums of the catalysts were tested by Raman spectrometer (Renishaw Via) within a wavelength range of 500 ~ 2500 cm^{-1}. X-ray photoelectron spectroscopy (XPS) was performed on a Thermo Scientific K-Alpha model instrument to determine the elemental valence of catalysts. Specific surface area and N_2 adsorption–desorption isotherms were calculated using the Brunauer-Emmet-Teller (BET) method on a Micromeritics ASAP 2460 instrument. The BET surface area of four catalysts were determined by N_2 adsorption–desorption at 77 K. The mass change of the catalysts was measured using a microwave thermogravimetric analyzer (MTGA, WSK12) to detect catalyst stability. Microwave thermogravimetry was used to test the stability of Fe/N-AC at 100 % power for 20 min.

2.3. Microwave-assisted hydrogenolysis experiment

The experiments of microwave-assisted hydrogenolysis of lignin were carried out in Galanz household microwave oven (G80F20CN2L-B8), which has a maximum power of 700 W, with a gradient of 70 W. The experimental setup is demonstrated in Fig. 1**b**. N_2 was continuously passed at a flow rate of 200 mL·min^{-1} to maintain an inert atmosphere. MeOH, EtOH, i-PrOH and their mixed solvents were used as hydrogen-donor solvents, respectively, which were delivered to the reactor through a gas-washing bottle. The gas-washing bottle containing the hydrogen-donor solvents was connected to N_2 bottle, with the flow rate of hydrogen-donor solvents also being 200 mL·min^{-1}. The microwave power and reaction time were determined based on the temperature rise curves of lignin and catalyst. Lignin (2 g) and the catalyst (1 g) were placed in the quartz reactor separated by a quartz plate, and microwave-assisted hydrogenolysis of lignin was carried out for 30 min at a power of 350 W. Bio-oil from the condenser was passed through the gas chromatography-mass spectrometry (GC–MS) analyzer for detection of the components after the operations of extraction, filtration, and spin evaporation, as shown in Fig. 1**c**. After drying, bio-gas was analyzed for

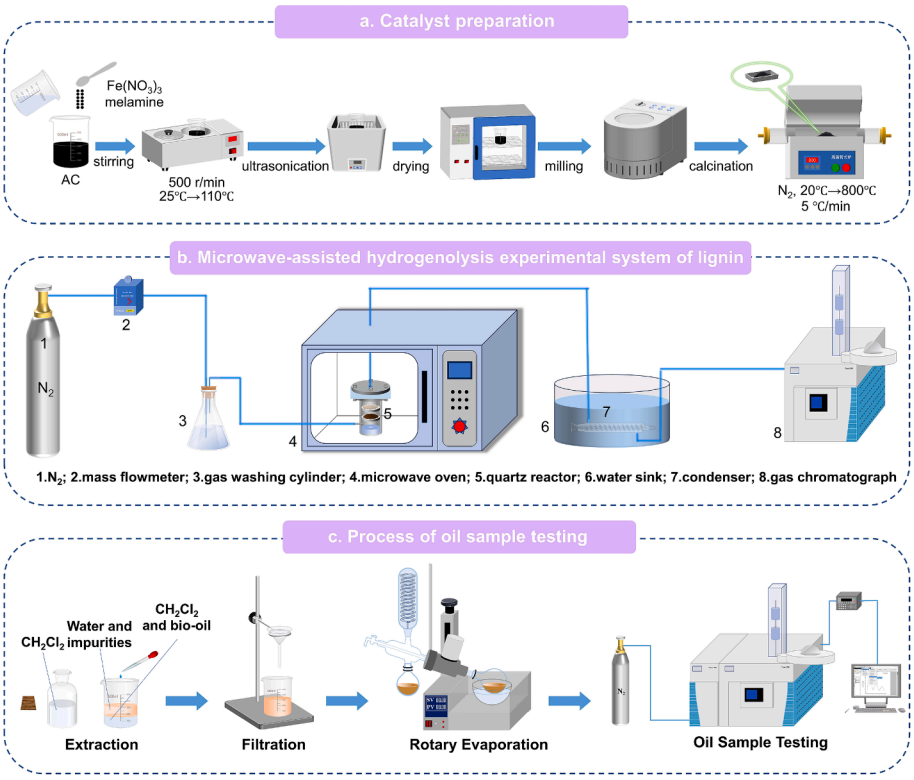

Fig. 1. Diagram of experimental setup.

its components by gas chromatography, and the mass of bio-gas was calculated to obtain the gas yield by Eq.(1). The mass of quartz reactor before and after the hydrogenolysis reaction was weighed to determine the bio-char yield. The mass difference before and after the hydrogenolysis reaction is used by subtraction method to determine the mass of bio-oil, thereby establishing its yield. In addition, energy conversion efficiency analysis, microwave thermogravimetric and conventional thermogravimetric analyses of lignin were performed, as detailed in the supporting information.

The mass of each gas is obtained from Eq. (1):

$$m_i = \frac{S_i}{S_{N_2}} \times v_{N_2} \times T \times \rho_{gas} \tag{1}$$

where m_i is the mass of ith gas in the bio-gas, g; S_i is the peak area of ith gas in the bio-gas; S_{N2} is the peak area of N_2; v_{N2} is the flow rate of N_2, 200 mL·min^{-1}; T is the working time, 30 min; ρ_{gas} is the density of each gas component, kg·m^{-3}.

The yield of each gas is found according to Eq. (2):

$$Y_i = \frac{m_i}{m_{gas}} = \frac{m_i}{\sum_{i=1}^{n} m_i} \times 100\% \tag{2}$$

where Y_i is the yield of ith gas in the bio-gas, %; m_{gas} is the total mass of bio-gas, g.

The formulae for three-phase products yields are Eqs. (3)-(5), respectively.

$$Y_{gas} = \frac{m_{gas}}{m_{total}} \times 100\% \tag{3}$$

$$Y_{oil} = \frac{m_{oil}}{m_{total}} \times 100\% \tag{4}$$

$$Y_{char} = \frac{m_{char}}{m_{total}} \times 100\% \tag{5}$$

where Y_{gas}, Y_{oil}, and Y_{char} denote the yield of bio-gas, bio-oil and bio-char, respectively, %; m_{gas}, m_{oil}, and m_{carbon} denote the total mass of bio-gas, bio-oil, and bio-char, respectively, g; and m_{total} denotes the total mass of lignin hydrogenolysis product, g.

2.4. Calculation method and model

The path of lignin hydrogenolysis was calculated by CASTEP module of Materials Studio 2020. In order to simplify calculation, a model of N-doped AC supported Fe catalyst without considering the carrier was established as basic catalyst model. The model was calculated by generalized gradient approximation (GGA) and Perdew-Burke-Ernzerhof (PBE) energy functional. The catalyst structure was optimized to ensure calculation accuracy, based on energy difference less than 2×10^{-5} eV and self-consistent field (SCF) convergence standard of 2×10^{-6} eV. The structure and energy of initial state (IS) and final state (FS) were also optimized in a similar manner. After the above optimization, the absorption energy of all the molecules involved in the process of lignin hydrogenolysis was calculated, following the equation of Eq. (6). Lastly, the configuration with the lowest energy was selected to find out transition state (TS) by using the method of complete linear synchronization and quadratic synchronization transformation (LSQ/QST). Taking into account breakage ways of the main chemical bonds in reactants, three likely paths were proposed in this work. The spin polarization of the electron during the calculation of the three paths was assumed to be colinear.

$$E_{ad} = E_{total} - (E_{catalyst} + E_{speices}) \tag{6}$$

where $E_{catalyst}$ is the energy of catalyst, $E_{speices}$ is the energy of active molecules, and E_{total} is the energy of active molecules adsorbed on catalyst.

3. Results and discussion

3.1. Catalyst characterization

In order to study the effect of Fe loading and nitrogen doping on catalyst crystals and carbon structures, AC and catalysts were characterized by XRD (Fig. 2**a**) and Raman (Fig. 2**b**). It is noticed that the carbon diffraction peak of samples is exhibited at around 26.4°. By comparison, the intensity of carbon diffraction peaks of N-doped AC catalysts is notably reduced and more defect sites were produced, causing the destruction of carbon mesh plane to lower the graphitization degree of catalysts [26]. This is further confirmed by Fig. 2**b**, in which the I_D/I_G of the Fe/AC, N-AC and Fe/N-AC increases from 0.791 to 0.981, 1.122 and 1.298, respectively. The decrease of graphitization degree indicates an increase of defect structures in AC, favoring the loading and dispersion of Fe components into the catalysts. The reason behind this is that the carbon nitride precursor volatilizes during the second phase (600 ~ 800 ℃) of preparing catalyst, resulting in the formation of more defect structures within the catalyst [27]. Meanwhile, it is found that the g-C_3N_4 characteristic peak appears near 27.4° for N-AC_{600} catalyst but not for N-AC_{800} catalyst, and the Fe_3N characteristic peak is found at near 43.6° for Fe/N-AC, indicating that N element is successfully doped into AC. This is due to the thermal cleavage of $C_3H_6N_6$ produces g-C_3N_4 at 600 ℃ [28,29]. When calcination temperature reaches 800 ℃, g-C_3N_4 decomposes to etch the carbon skeleton and increases the defect structure of catalysts, allowing Fe components dispersed uniformly.

As shown in Fig. 2**c**, it is noticed that N-AC_{600} exhibits type-I isotherms, indicating the presence of only micropores in the catalyst. Micropores limit the adsorption and desorption of lignin intermediates on the surface of active sites, thereby preventing lignin intermediates from contacting with active sites. This phenomenon arises from the thermal cleavage of $C_3H_6N_6$, which produces carbon nitride precursors that cover the pore structure of support. The other catalysts are type-IV isotherms, and a clear type-H4 hysteresis appears when $P/P_0 \geq 0.5$, indicating the presence of mesoporous structures in the catalysts. The

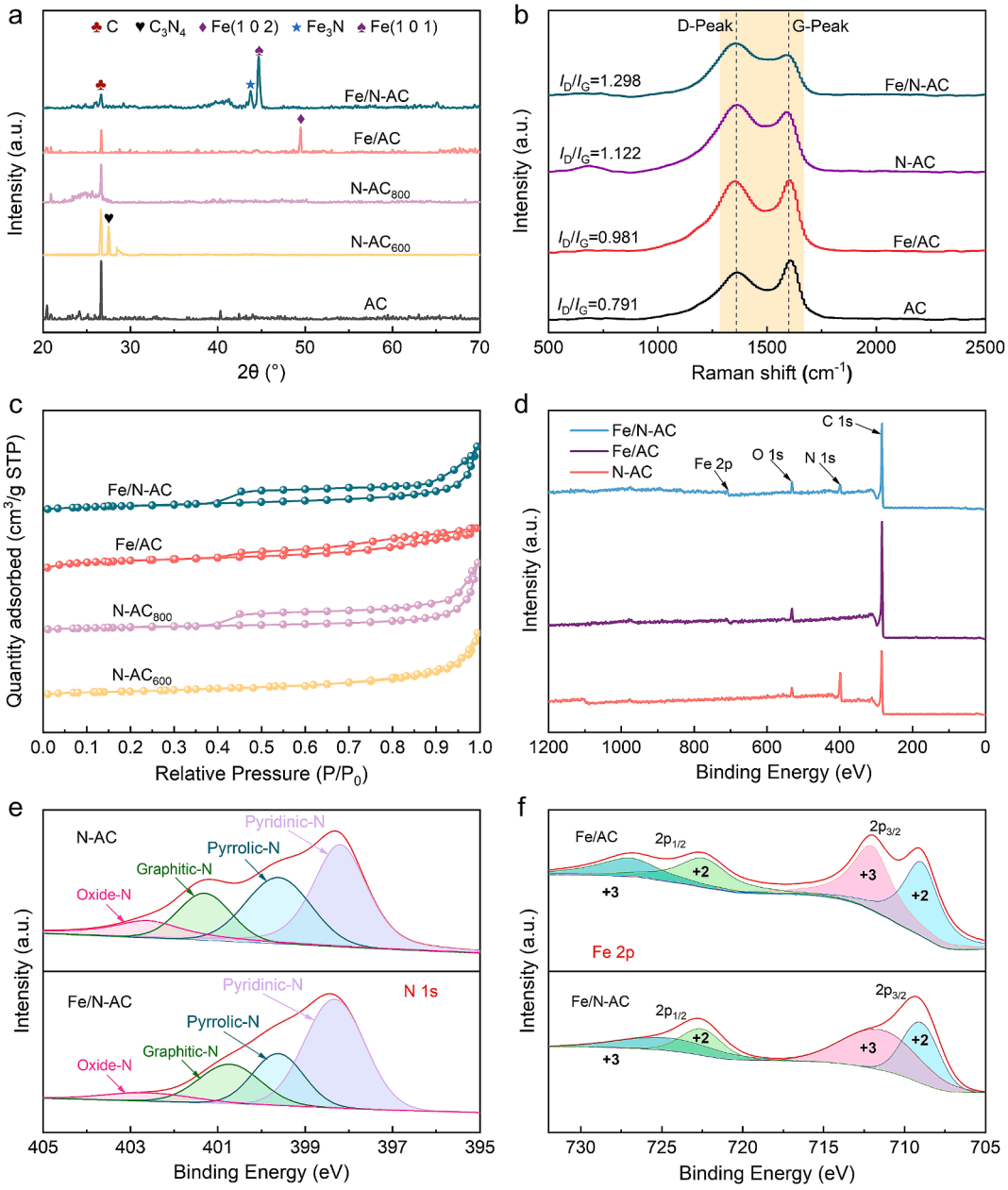

Fig. 2. Characterization of as-prepared samples. a. XRD; b. Raman; c. N_2 adsorption–desorption isotherm of catalysts; d-f. XPS.

reason behind this is that pyrolysis of carbon nitride precursor produces carbon and nitrogen radicals to etch the carbon skeleton structure after 800 ℃, which improves the specific surface area of catalysts to make more active sites attached to the pore structure [27]. The N-AC and Fe/N-AC were further analyzed by XPS (Fig. 2**d**, Fig. 2**e** and Fig. 2**f**), from which it can be observed that the high-resolution energy spectrum of Fe 2p is divided into four peaks, including $Fe^{2+}2p_{1/2}$, $Fe^{2+}2p_{3/2}$, $Fe^{3+}2p_{1/2}$ and $Fe^{3+}2p_{3/2}$. This is consistent with the valence of the Fe-containing catalysts in XRD. As depicted in Fig. 2**e**, the different N species can be distinguished into pyridinic-N, pyrrolic-N, graphitic-N and oxide-N, according to the binding energy of 398.5 eV, 399.2 eV, 401.5 eV and 403.5 eV. Among them, the peak area of pyridinic-N is the most prominent, suggesting that N element in the catalyst primarily exists in the form of pyridinic-N. Pyridinic-N predominantly resides in the defect structure of the support, coordinating with Fe through the Fe-N_x bonds and enhancing the dispersion of Fe [30,31].

3.2. Product analysis

Fig. 3 shows the three-phase product yields and components of bio-gas of microwave-assisted hydrogenolysis of lignin under different hydrogen-donor solvents and catalysts. As depicted in Fig. 3**a**, the bio-oil yield is only 10.9 wt% and the bio-char yield reaches as high as 50.67 wt % without hydrogen-donor solvents, indicating that the branched chains and functional groups of lignin primarily undergo thermal reforming to result in the high degree of carbon gasification [32]. Under the single solvent, the bio-oil yield increases to 23.2–28.91 wt% and the bio-char yield decreases to 34–40 wt%. In details, EtOH exhibits the best hydrogen-donor performance with the yields of bio-oil, bio-char and bio-gas of 28.91 wt%, 34.0 wt% and 37.09 wt%, respectively, attributed to the activation of H* for lignin intermediates. This indicates that hydrogen-donor solvents can inhibit the condensation of lignin intermediates to increase bio-oil yield [21]. The influence of different hydrogen-donor solvents on the lignin hydrogenolysis products is mainly dependent on the theoretical hydrogen-donor capacity and the lignin solubility of the different solvents. The former determines the difficulty of hydrogen radical (H*) generation, while the latter affects the degree of lignin crystallinity reduction. Through comparison, it is noticed that MeOH has the greatest BDE of C-O bond, enhancing the difficulty of H* generation, while i-PrOH exhibits the least lignin solubility (**Fig.S2** and **Table S1**), meaning the lowest ability to reduce lignin crystallinity [17]. As a consequence, the moderate theoretical hydrogen-donor capacity and lignin solubility resulted in the best hydrogenolysis performance in the EtOH, especially from the point of view of the bio-oil production.

The mixed solvents lead to a further increase in the yield of bio-gas or bio-oil. The best hydrogen-donor performance among the mixed solvents is observed with EtOH/i-PrOH, leading a decrease in bio-char yield to 31 wt%, while bio-oil and bio-gas yields increase to 31.5 wt% and 37.5 wt%, respectively. The reason behind this may be that i-PrOH as a secondary alcohol shows higher activity in dehydrogenation than primary alcohols over the catalyst's surface. Meanwhile, the mixture of alcohol solvents increases the concentration of hydrogen radicals to produce stronger activation for specific bonding in lignin and is helpful to reduce the polymerization of lignin. Thus, EtOH/i-PrOH is selected as hydrogen-donor solvents for subsequent experiments. As seen in Fig. 3**c**, the yields of bio-oil, bio-gas and bio-char in absence of catalyst are 31.5 wt%, 38.5 wt% and 30 wt%, respectively. The introduction of catalysts manifests as an increase of bio-oil yield and a decrease in the yield of bio-char and bio-gas. The yield of bio-oil increases to 40.3 wt%

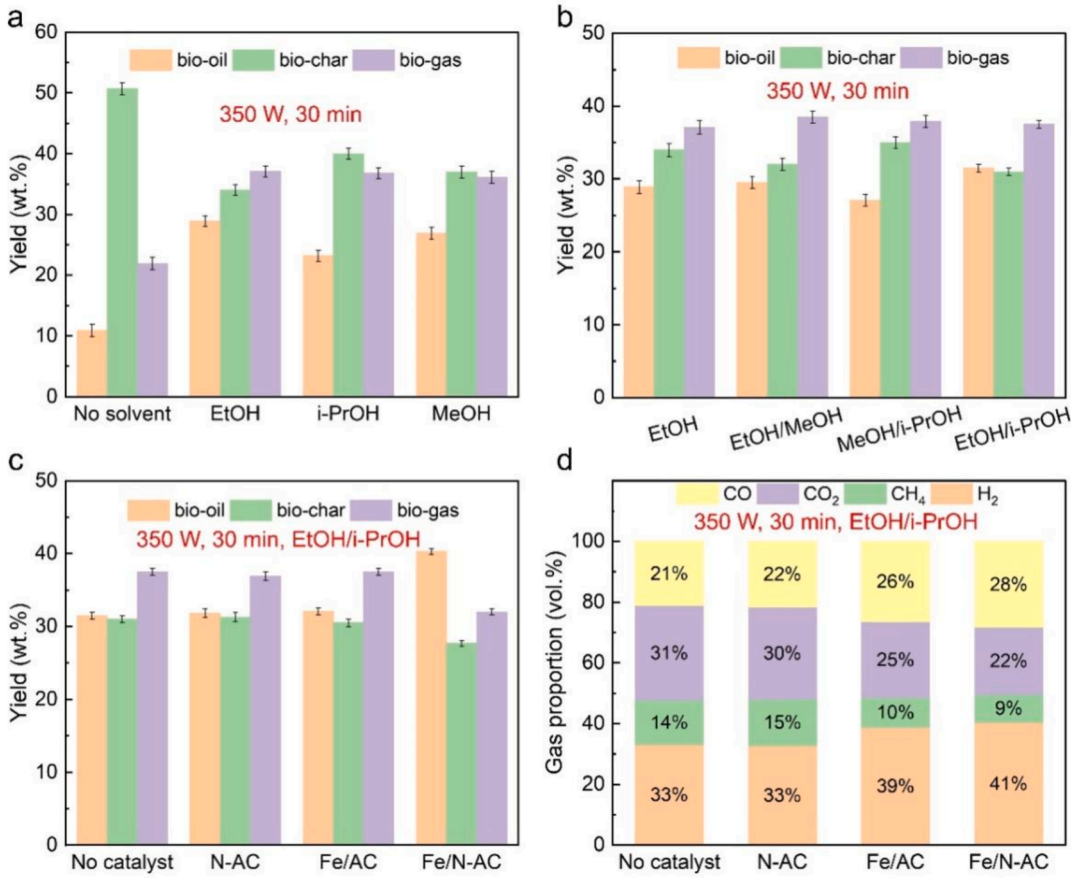

Fig. 3. Three-phase product yield and gas composition. a. Three-phase product yield in single solvent; b. Three-phase product yield in mixed solvent; c. Three-phase product yield under catalyst and mixed solvent; d. Gas composition under catalyst and mixed solvent.

(for Fe/N-AC) while the bio-gas yield decreases to 32 wt%, accompanied by a marked decrease in bio-char yield by 3.8 wt%. This suggests that the Fe-N_x bonds of Fe/N-AC adsorbs a high amount of H^+ to accelerate the breakage of C-C and C-O bonds in lignin, promoting the enhancement of liquid-phase products. As illustrated in Fig. 3**d**, Fe/N-AC increases the volume fraction of H_2 and CO to 40.5 wt% and 28.3 wt%, respectively, compared to Fe/ AC and N-AC, while reducing the volume fraction of CH_4 and CO_2. This may be due to the reforming reaction ($CH_4 + CO_2 \rightarrow 2CO + 2H_2$) of CH_4 and CO_2 generated by functional groups under the action of Fe/N-AC, where functional groups are mainly from $–OCH_3$ and $–CH_3$ on the branched chains of lignin molecules [32]. CH_4 is mainly derived from $–CH_3$, which is hydrogenated to form CH_4 in the presence of H*. The breakage of C-O bonds in lignin makes the production of CO_2. In addition, it can be observed from Fig. 3**d** that the influence of N-AC and Fe/AC on the distribution of bio-gas is relatively weak, indicating that the metal-support effect of Fe-N_x bonds in Fe/N-AC is an important factor of bio-gas catalytic reforming.

The GC–MS spectra of bio-oils and FTIR spectra of bio-chars under different catalysts were analyzed, as shown in Fig. 4. It can be seen from Fig. 4**a** that there are mainly 13 liquid-phase products from microwave-assisted hydrogenolysis of lignin. The characteristic peaks of bio-oil are relatively chaotic without catalyst and does not have obvious selectivity. The characteristic peak intensity of phenol is gradually enhanced after introducing catalysts, indicating that the catalyst can effectively depolymerize lignin intermediates and monomers to produce products with smaller atomic number (such as phenol). The characteristic peak intensity of phenol is significantly increased with Fe/N-AC, since the metal-support effect of Fe-N_x bond makes lignin intermediates break C_{Ar}-OCH_3 bonds tendentially. The bio-oils are further categorized according to the type of functional groups, as shown in Fig. 4**b**. The introduction of catalyst leads to a gradual increase of phenolic compounds yield, reaching 98.0 % in the presence of Fe/N-AC, accompanied by a decrease of aldehydes, esters and other by-products. This indicates that the synergistic effect of catalyst and H* further enhances the extent of lignin hydrodeoxygenation [33].

As observed in Fig. 4**c**, the yield of phenol increases with the upgrading of catalysts, and the yield magnitude of phenol on different catalysts follows the following order: Fe/N-AC > Fe/AC > N-AC > no catalyst. Fe/N-AC attains the largest phenol yield of 38.71 %, indicating its high selectivity for breaking C_{Ar}-O bonds. In addition, the yield of catechol under Fe/AC is 23.54 %, indicating its tendency to break C_R-O bonds of methoxy. Catechol is fully transformed under Fe/N-AC, further demonstrating that Fe/N-AC has high selectivity for breaking the C_{Ar}-O bonds to increase the phenol yield. This is because the adsorption capacity of Fe/N-AC is stronger than that of N-AC and Fe/AC, which prolongs the residence of lignin intermediates and promotes the hydrodeoxygenation of lignin. Meanwhile, both Fe/N-AC and N-AC have high selectivity for 4-Ethylphenol with 13.83 % and 17.85 %, respectively. The reason behind this may be from two sides: On the one hand, the defect sites that located at N-doped AC catalysts can anchor the Fe component (metal effect), providing catalytic sites for lignin hydrogenolysis with strong adsorption of oxygenated functional groups on the benzene ring. On the other hand, the display of electronegativity around N element is capable of adsorbing H^+ and H*, which are able to further activate C-C and C-O bonds while hydrogenating lignin intermediates [34,35]. As illustrated in Fig. 4**d**, the –CH vibrational peak at 2937 cm^{-1} disappeared in the presence of catalysts. This reveals that the use of catalysts promotes the breakage of branched chains, enhancing preliminary depolymerization of lignin. It was further noticed that the intensity of C-O stretching vibrational peaks at 1040 and 1130 cm^{-1} evidently depressed, especially in the presence of Fe/N-AC. This is a convincing proof that Fe/N-AC effectively promotes the breakage of C-O bonds in lignin.

The results in Table 1 showed that Fe/N-AC considerably increased

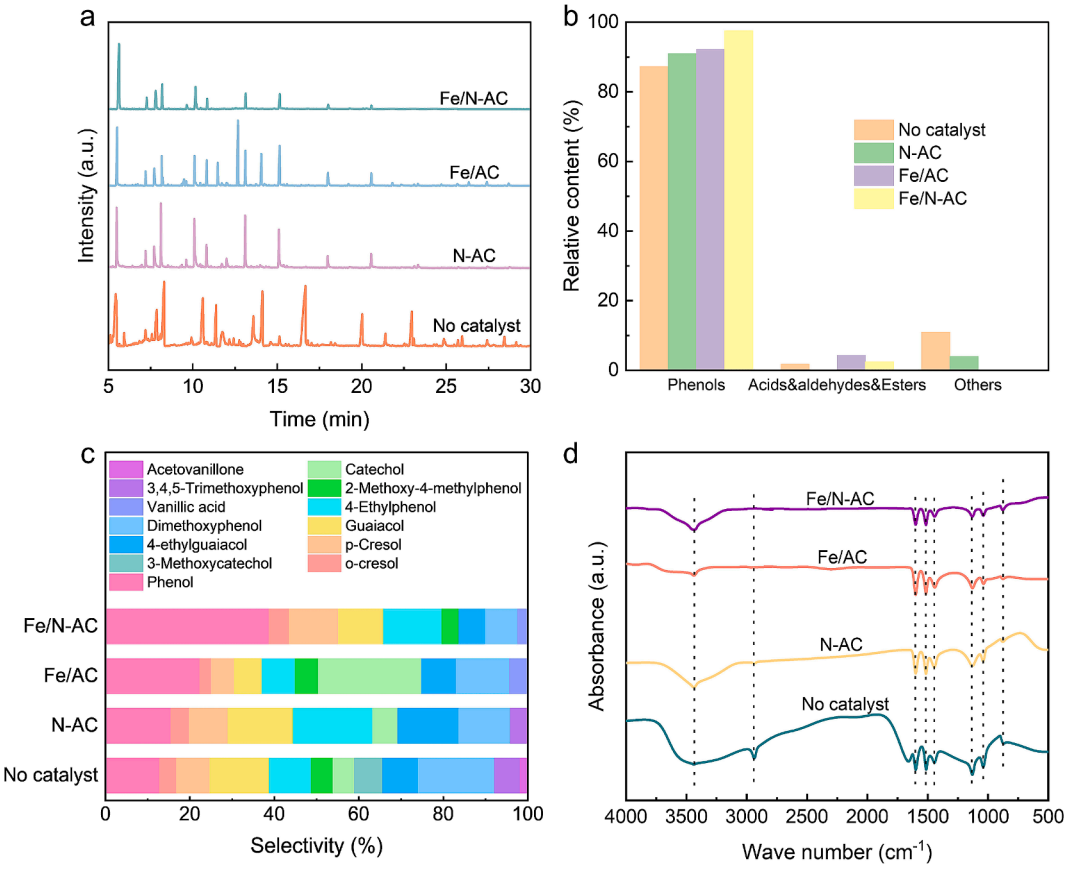

Fig. 4. Analysis of bio-oil and bio-char. a. GC–MS mass spectrometry; b. Relative content; c. Distribution of bio-oil; d. FTIR of bio-char.

Table 1
Comparison of phenol selectivity.

Catalysts	Conversion methods	Phenol selectivity (%)	Reference
Fe/N-AC	Microwave heating	38.71 %	This work
Fe-MoS_2/CMF	Microwave heating	30.01 %	[4]
Ni-Fe/$MgSiO_3$	Hydrothermal liquefaction	0.79 %	[36]
Fe/C	Hydrothermal liquefaction	6.4 %	[37]

the phenol selectivity (38.71 %) of microwave hydrogenolysis of lignin, compared with the other Fe-based catalysts. In the literature, the greatest phenol selectivity was 30.01 % in the presence of Fe-MoS_2/CMF [4]. For this superiority, it can be explained from the two sides. For one thing, the quickness and selectivity of microwave heating reduced the occurrence of side reactions in the process of lignin hydrogenolysis, compared to the hydrothermal liquefaction; for another, nitrogen doping provides a stable coordination environment for carbonaceous catalysts so that the metal components can be better anchored, providing the better catalytic activity for lignin hydrogenolysis into phenol products.

3.3. Cycle stability

The stability of Fe/N-AC was tested five times at 350 W, as shown in Fig. 5. As seen in Fig. 5**a**, the selectivity of phenolic compounds is still more than 90 % after five cycles, indicating that the Fe/N-AC is able to maintain the high catalytic activity. This may be attributed to the layering of catalyst with lignin in the quartz reactor, extending the catalyst life by avoiding the direct contact between the obtained biochar and catalyst. Microwave thermogravimetric analysis was performed in successive experiments to assess the thermal stability of the catalysts, as shown in Fig. 5**b**. The three catalysts retain more than 90 % of their weights after 20 min, indicating that three catalysts can remain stable at prolonged high temperature. This is because volatile substances, organic compounds, and oxygenated functional groups present

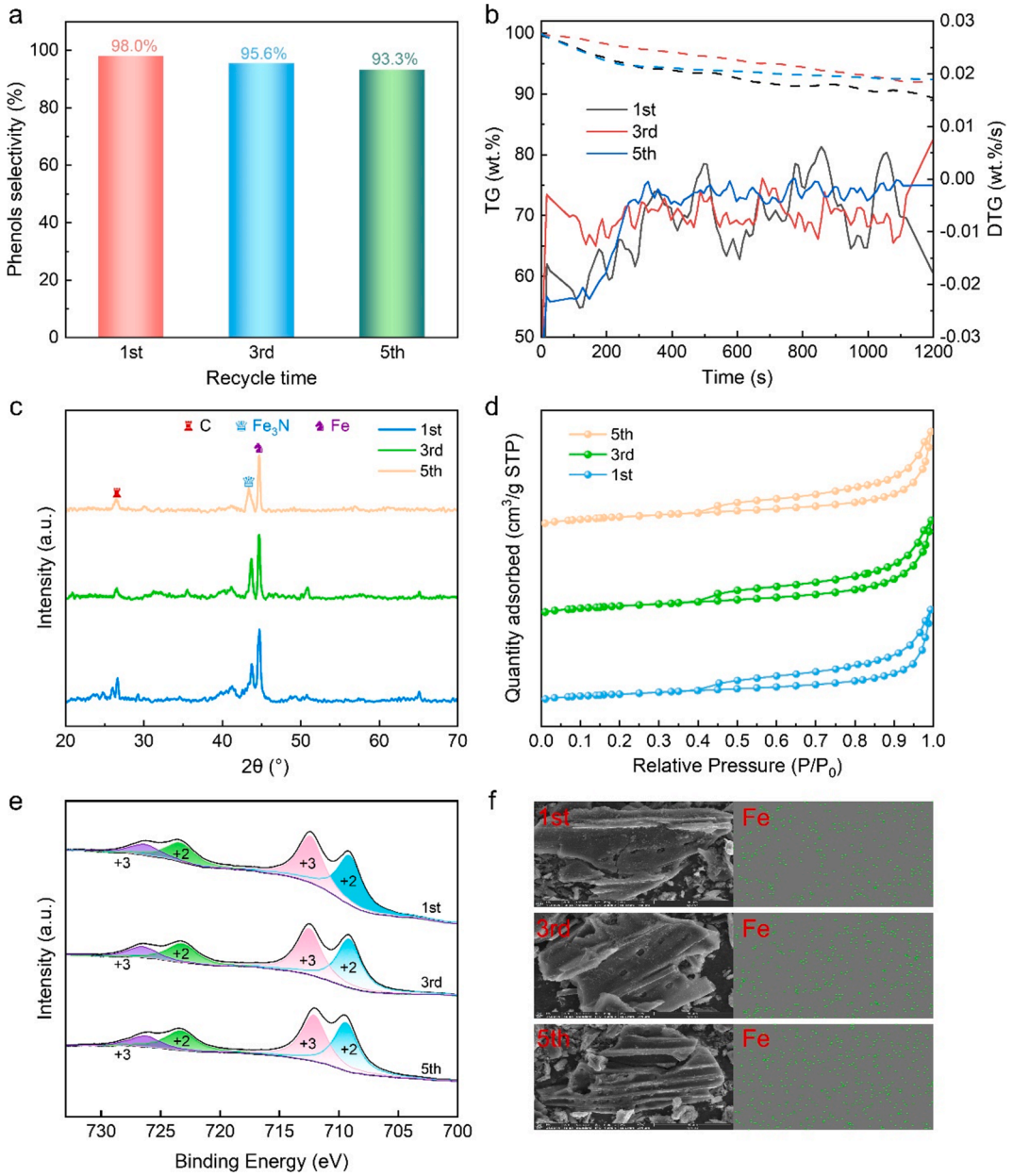

Fig. 5. Recycling stability of the used catalysts. a. Phenols selectivity; b. TG and DTG; c. XRD; d. N_2 adsorption–desorption isotherm; e. XPS; f. SEM and EDS.

in the catalyst have been largely removed during high-temperature calcination [38]. Fig. 5**c** shows the XRD spectra of three catalysts. Compared with fresh catalysts, the characteristic peaks of the used catalysts do not change significantly, indicating that the used catalysts hardly undergo the agglomeration of metal components after several cycles of microwave-assisted hydrogenolysis of lignin. This may be because carbonaceous material can occur partial graphitization under high temperature, forming relatively stable N-doped AC structures that make the active components difficult to aggregate and deactivate [39].

The mesoporous structure of catalysts remains stable after five cycles in Fig. 5**d**, indicating that there are not significant carbon deposits to cause pore clogging for the used catalysts. This is attributed to the elimination role of deposited carbon under the microwave irradiation, where majority of deposited carbon is eliminated by CO_2 gasification [40]. The catalysts can maintain stable physicochemical properties after five cycles, indicating that the metal-support effect of Fe-N_x bonds effectively ensures the thermal stability of the catalyst and microwave effectively suppresses the generation of carbon deposits. Fig. 5**e** shows the XPS spectra of three catalysts after five cycles, from which it was witnessed that the valence state of iron still remained divalent and trivalent, without reduction to elemental iron. This means there is no evident leaching of Fe from the catalyst after five cycles. The SEM and EDS images of Fe/N-AC in Fig. 5**f** further demonstrates this conclusion. As it is shown, the pores of Fe/N-AC were not obviously clogged after five cycles, and also the Fe was uniformly dispersed on the catalyst, with no noticeable signs of Fe leaching. The above results state that the issue of Fe leaching for the catalyst of Fe/N-AC during the hydrogenolysis reaction has well been addressed, and this is one of the reasons why the catalyst shows an excellent cycle stability for lignin microwave hydrogenolysis.

3.4. Advantages of microwave-assisted hydrogenolysis

Conventional and microwave thermogravimetric analysis of lignin hydrogenolysis is shown in Fig. 6**a**. It is observed that under microwave irradiation, the mass retention rate of lignin stabilizes quickly, whereas the mass retention rate of lignin levels off after 20 min under conventional hydrogenolysis. The mass retention rate of lignin during microwave-assisted hydrogenolysis is lower than that of conventional hydrogenolysis, indicating that lignin is more readily depolymerized under microwave irradiation. Fig. 6**b** and Fig. 6**c** present the kinetic curves for the microwave-assisted hydrogenolysis and conventional hydrogenolysis of lignin, respectively. The activation energy for conventional hydrogenolysis of lignin is 93.57 kJ·mol^{-1}, whereas for microwave-assisted hydrogenolysis of lignin, it is 33.21 kJ·mol^{-1}. This is attributed to the internal-to-external heating mechanism of microwave, which enables bonds break more thoroughly and further hydrogenation. The energy conversion efficiency (η_2) of microwave energy into effective thermal energy is calculated as 36.71 % by using the formula in the appendix. Further, it is shown that the energy consumption for microwave-assisted lignin depolymerization is only 3.68 % of that for conventional depolymerization under the same power and temperature [41]. This indicates that Fe/N-AC possesses excellent microwave absorption properties to reduce the activation energy of hydrogenolysis reaction, which has the significant energy-saving effect for the whole reaction process.

3.5. Possible pathway of guaiacol hydrodeoxygenation

3.5.1. Catalyst electronic structure analysis

In order to analyze the impact of nitrogen doping on the catalyst's electronic structure, density of states and electrostatic potential

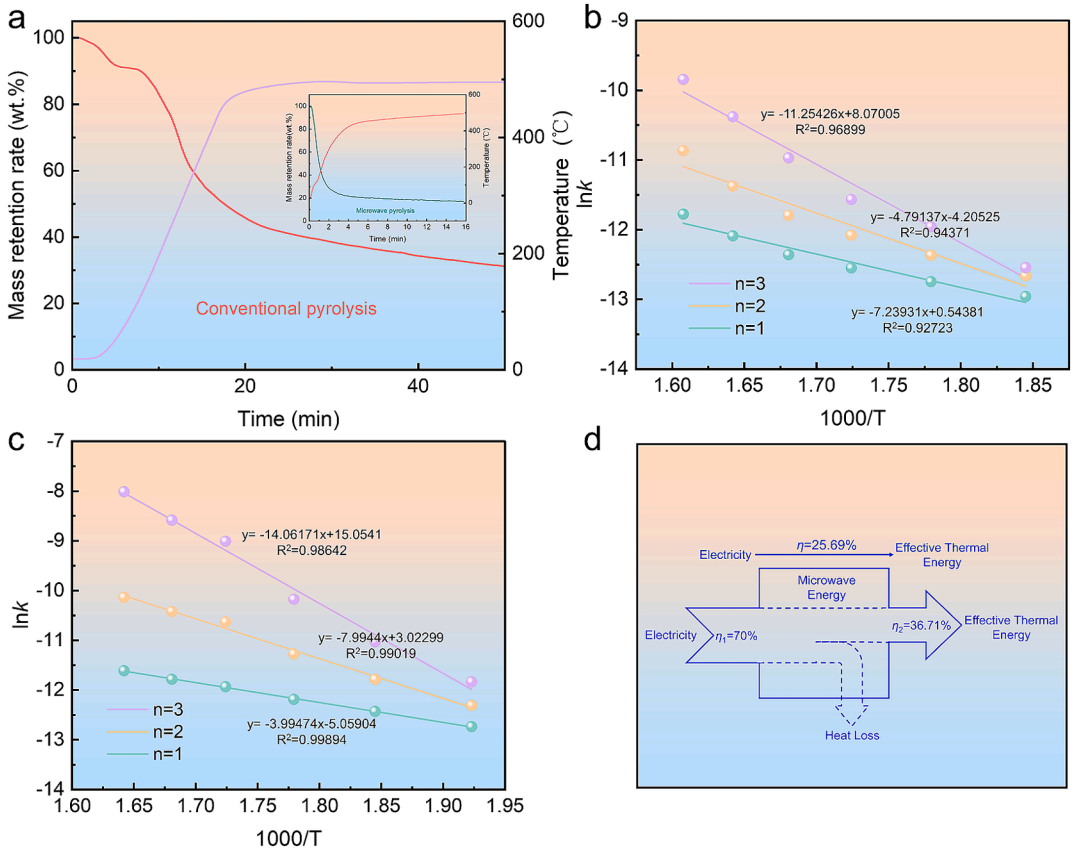

Fig. 6. Conventional and microwave thermogravimetric analysis of lignin hydrogenolysis. a. TG; b. Kinetic curves for conventional hydrogenolysis; c. Kinetic curves for microwave hydrogenolysis; d. Energy conversion efficiency.

distributions were calculated for catalyst models, as shown in Fig. 7. The calculation results show that the Fe/N-AC conduction and valence bands are mainly composed of the 2p and 3d orbitals of Fe, the 3p orbital of N and the 2p orbital of C. As shown in Fig. 7**b-7d**, the resonance peaks appear between the 2p orbital of C and the 3d orbitals of Fe, indicating that the orbitals of C and Fe overlap to form Fe-C bonds. Simultaneously, the resonance peaks between the 2p orbital of N and the 3d orbitals of Fe also indicate the presence of chemical bonding between N and Fe, that is, the Fe-N bonds. The formation of Fe-C and Fe-N bonds indicates that N-AC has an anchoring effect on Fe, which improves the dispersion of Fe. The defective sites of N-doped AC increases, facilitating better anchoring of Fe components. Meanwhile, the interaction between support and Fe modulates the electronic structure of Fe, enhancing the catalyst activity. The formation of Fe-N bonds strengthens the interaction energy between Fe and the support, imparting the thermal stability of the catalyst to reduce Fe aggregation.

Fig. 7**e** shows the electrostatic potential distribution of pyridinic-N. The reason to select pyridinic-N as the subject of simulation primarily stems from XPS testing, which reveals that N predominantly exists in the form of pyridinic-N. The N defect sites appear in dark blue color, signifying the negative potential around N element. This indicates that the defect sites can spontaneously attract Fe and generate Fe-N_x bonds. It confirms that the 2p orbitals of N and the 3d orbitals of Fe overlap to create the Fe-N bonds, as observed from Fig. 7**b** and Fig. 7**c**. As shown in Fig. 7**f**, the electrostatic potential distribution of Fe-N_3 shows electronegativity of N, which is favorable for its adsorption of H^+ and H* to promote lignin hydrodepolymerization. The elevation of H^+ and H* concentrations on the catalyst surface is bound to significantly increase the bio-oil yield. The positive electrostatic potential around Fe indicates that it can adsorb electronegative functional groups such as –CH_3, –OCH_3 and –OH on the branched chain of benzene ring, detaching them from benzene ring to speed up the hydrogenation of obtained intermediates. Overall, the synergistic effect generated by the N adsorption of H* and Fe removal of oxygenated functional groups increases the hydrodeoxygenation degree of lignin to increase the yield of phenol.

3.5.2. *Possible reaction pathway*

The bio-oils are primarily guaiacol-derived compounds in the hydrogenolysis experiments. Therefore, guaiacol is commonly used as a substrate for simulating lignin hydrogenolysis reactions, and its use helps eliminate the influence of structural variations among different lignin types on simulation results. As shown in Fig. 8**a**, it is calculated

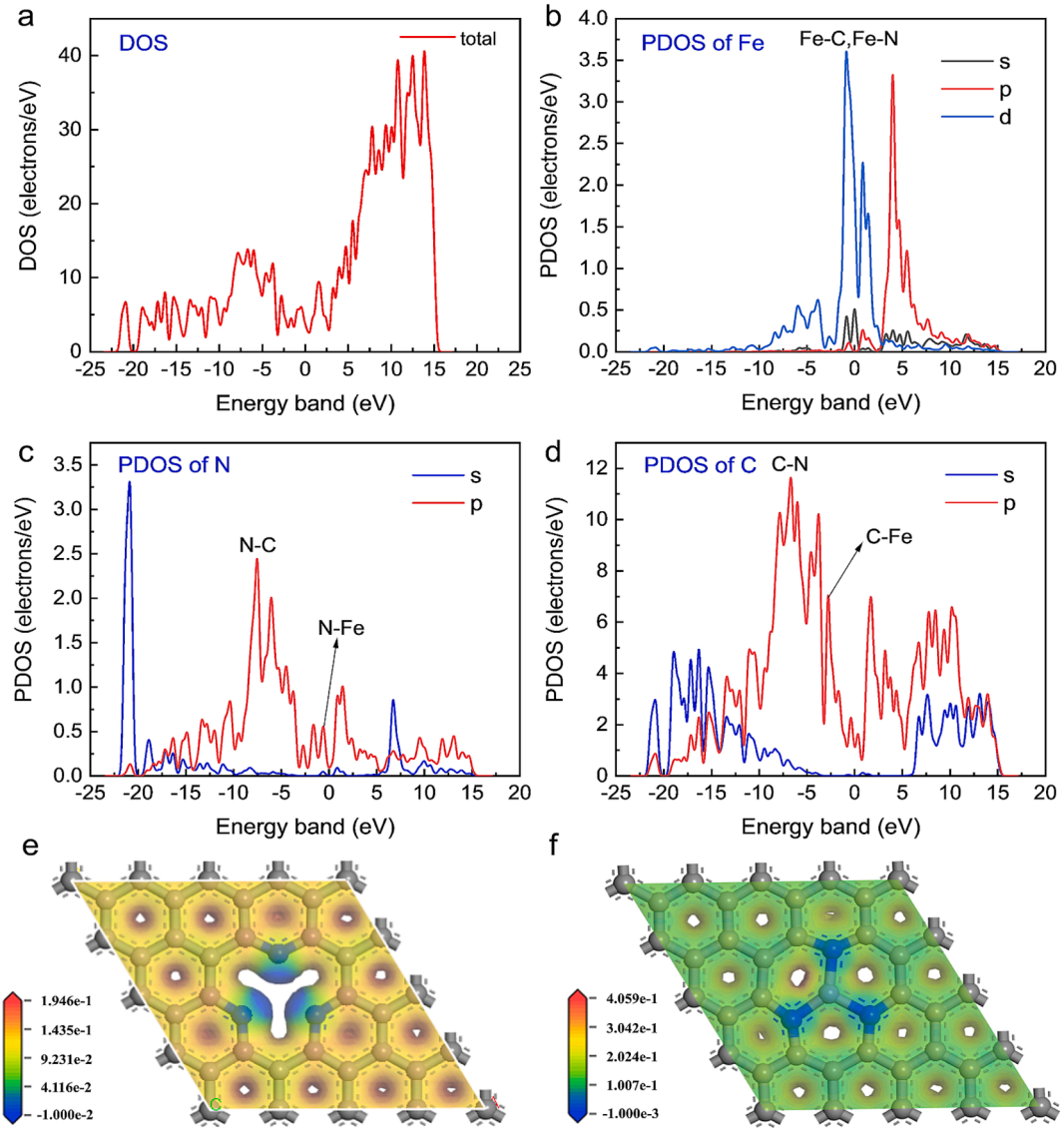

Fig. 7. Catalyst electronic structure analysis. a. Total DOS; b. PDOS of Fe; c. PDOS of N; d. PDOS of C; e. Electrostatic potential distribution of pyridinic-N; f. Electrostatic potential distribution of Fe-N_3.

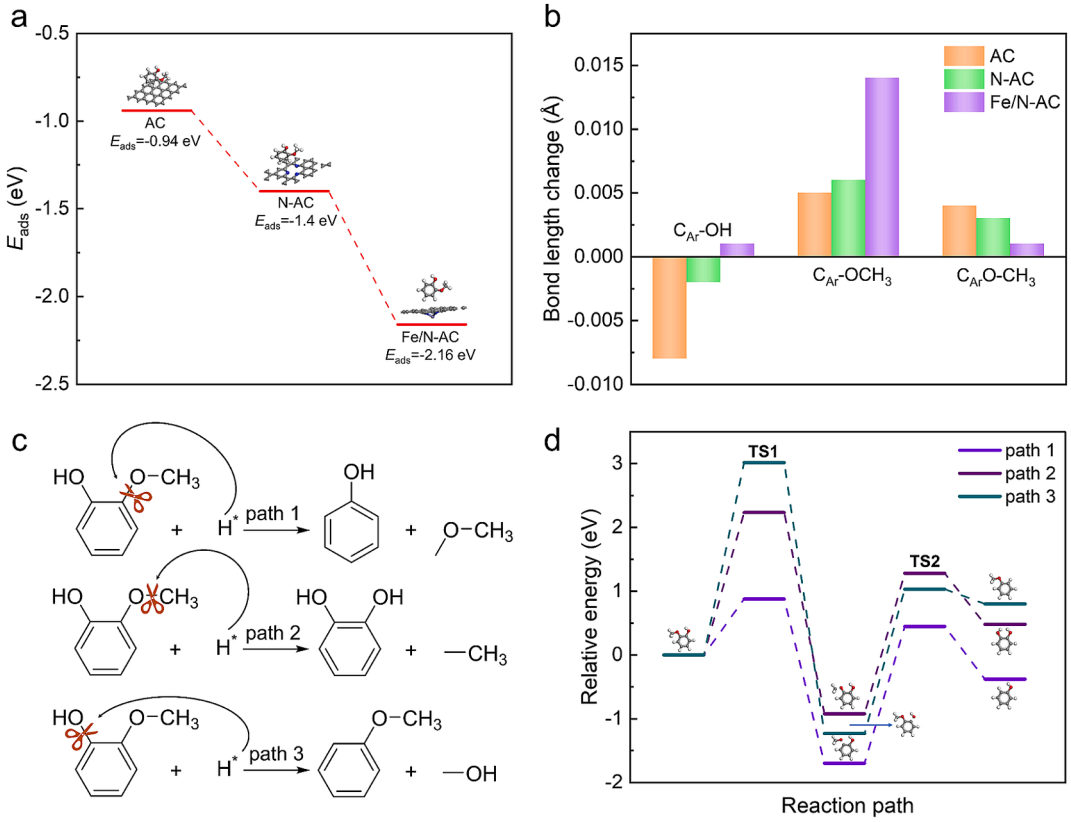

Fig. 8. Possible pathways and energy barriers over different catalysts. a. Adsorption energy; b. Bond length change; c. Proposed reaction path; d. Energy barriers.

that the adsorption energies of AC, N-AC and Fe/N-AC for guaiacol are −0.94, −1.40 and −2.16 eV, respectively. Compared with AC and N-AC, the adsorption energies of Fe/N-AC for guaiacol are enhanced by 129.79 % and 54.29 %, respectively, attributed to the synergistic effect of Fe loading and N doping to enhance the adsorption performance for guaiacol. This conclusion is also verified in **Fig.S3**, with the distance of guaiacol being closest to Fe/N-AC after adsorption. Fig. 8**b** shows the changes of oxygenated bonds length after adsorption of guaiacol in the presence of AC, N-AC and Fe/N-AC. It can be seen that the C_{Ar}-OCH_3 bond length stretches the longest, indicating that the guaiacol tends to be demethoxylated in the presence of Fe/N-AC. It is found that the catalysts have no effect on the stretch of C_{Ar}-OH and even the C_{Ar}-OH bond lengths shorten in the presence of AC and N-AC, indicating that –OH is difficult to remove from benzene ring to form anisole.

Taking into account breakage ways of the oxygenated bonds mentioned above, three possible paths are proposed for guaiacol hydrogenolysis with the use of Fe/N-AC, as shown in Fig. 8**c**. The above pathways can be referred to as guaiacol demethoxylation, guaiacol methoxy demethylation, and guaiacol dehydroxylation, respectively, whose target products are phenol, catechol, and anisole, respectively. As indicated in Fig. 8**d**, the energy barriers for breaking C_{Ar}-OCH_3, $C_{Ar}O$-CH_3, and C_{Ar}-OH are 0.877, 2.233 and 3.018 eV, respectively, presenting a tendency of breaking C_{Ar}-OCH_3 under Fe/N-AC, which is in agreement with the results obtained in Fig. 8**b**. For the obtained intermediates, there are hydrodeoxygenation by H* derived from hydrogen-donor solvents into the target products of phenol, catechol and anisole, with the energy barriers of 2.144, 2.202, and 2.264 eV, respectively. This suggests that the rate-determining step of guaiacol hydrodeoxygenation is dominated by TS1. Based on these calculated results, it is derived that path 1 is the most likely path for lignin hydrodepolymerization in presence of Fe/N-AC. Subsequent work can improve the catalyst to increase the capability of breaking bonds in path 1, in terms of loading bimetals, changing doping elements and changing catalyst supports [4,12,42].

In the microwave-assisted hydrogenolysis of lignin process, microwave irradiation on the bed layer induces lignin hydrogenolysis at high temperatures to generate small molecular gases (CH_4, H_2, CO_2, CO). Under the catalysts and microwave irradiation, EtOH and i-PrOH are converted into acetaldehyde and acetone, respectively, with the generation of H* and H^+. Simultaneously, H_2 in the bio-gas becomes H* and H^+ under microwave irradiation, which also promotes lignin hydrogenolysis to a certain extent. Next, H* and H^+ are absorbed onto the catalyst surface, since the defect sites in the pyridinic-N and the N atoms on Fe-N_x bonds exhibit electronegativity. Meanwhile, Fe^{2+} and Fe^{3+} in the Fe/N-AC adsorb the oxygen-containing functional groups of intermediates to the catalyst surface. Ultimately, H^+ and H* activate and break the C-O bonds of lignin intermediates under the action of Fe/N-AC, undergoing a series of reactions such as dehydration, decarbonylation, decarboxylation and demethoxylation to produce monophenolic compounds including phenol.

4. Conclusions

In this study, a feasible strategy of nitrogen doping to promote the stability of N-doped AC supported Fe catalyst was proposed. The incorporation of N into the carbon structures ensured the uniform dispersion of Fe. Microwave-assisted hydrogenolysis of lignin using Fe/N-AC obtained the bio-oil yield of 40.30 wt% and the phenol compounds selectivity of 98.00 % in the presence of EtOH/i-PrOH. Cycling experiments revealed a phenolic selectivity of 93.3 % after five trials, a decrease of only 4.79 %, demonstrating an excellent cycle stability. The optimal pathway of lignin hydrogenolysis in presence of Fe/N-AC was proposed by DFT calculation.

It is reasonable to believe that the coupling of this catalyst with

microwave technology has a broad application for the disposal of industrial waste lignin and even lignocellulose into valuable chemicals. This ultimately changes the conventional lignin utilization method (i.e., combustion), greatly enhancing the economic value and environmental benefits of lignin utilization. In addition, the liquid and gaseous products derived from this method can be further converted into clean bio-fuels through catalytic upgrading, showing sustainably environmental benefits. In the future research, we will focus on the hydrogenolysis characteristics of various sources of lignin to investigate different bond breaking laws, developing new hydrogen-donor solvents to study the influence of hydrogen radical dynamic evolution on the intermediates and products of the hydrogenolysis process, as well as verifying the method universality of nitrogen doping for improving catalyst cycling performance.

CRediT authorship contribution statement

Junhao Cui: Writing – original draft. **Zhiyang Zhao:** Supervision. **Yongqi Ren:** Software. **Bailong Chen:** Methodology. **Chase Rheinlander:** Writing – original draft. **Antonio Xavier Moore:** Investigation. **Longzhi Li:** Writing – review & editing.

Declaration of competing interest

The authors declare that they have no known competing financial interests or personal relationships that could have appeared to influence the work reported in this paper.

Acknowledgements

This work has been supported by National Natural Science Foundation of China (No. 22172091), Natural Science Foundation of Shandong Province (ZR2021ME184).

Appendix A. Supplementary data

Supplementary data to this article can be found online at https://doi.org/10.1016/j.cej.2024.158001.

Data availability

No data was used for the research described in the article.

References

[1] Y.M. Questell-Santiago, M.V. Galkin, K. Barta, et al., Stabilization strategies in biomass depolymerization using chemical functionalization, Nat. Rev. Chem. 4 (6) (2020) 311–330.
[2] C. Zhang, F. Wang, Catalytic lignin depolymerization to aromatic chemicals, Acc. Chem. Res. 53 (2020) 470–484.
[3] C.F. Zhang, X.J. Shen, Y.C. Jin, et al., Sell a dummy: Adjacent functional group modification strategy for the catalytic cleavage of lignin β-O-4 linkage, Chem. Rev. 123 (2023) 4510–4601.
[4] W.L. Wang, J.L. Huang, Y.S. Fu, et al., A 3D porous Fe-MoS_2/CMF catalyst for high-efficient catalytic reforming of lignin vapor by microwave irradiation, Appl. Catal. B: Environ. 333 (2023) 122787.
[5] C.S. Lancefield, O.S. Ojo, F. Tran, et al., Isolation of functionalized phenolic monomers through selective oxidation and C-O bond cleavage of the β-O-4 linkages in lignin, Angew. Chem. 127 (1) (2015) 260–264.
[6] J. He, C. Zhao, J.A. Lercher, Ni-catalyzed cleavage of aryl ethers in the aqueous phase, J. Am. Chem. Soc. 134 (51) (2012) 20768–20775.
[7] C. Zhu, J.P. Cao, X.B. Feng, et al., Theoretical insight into the hydrogenolysis mechanism of lignin dimer compounds based on experiments, Renew. Energy 163 (2021) 1831–1837.
[8] J.P. Guo, F.J. Liu, L.L. Bie, et al., Selective cleavage of C-O bond in lignin and lignin model compounds over iron/nitrogen co-doped carbon supported Ni catalyst, Fuel 316 (2022) 123338.
[9] L.L. Bie, F.J. Liu, Z.M. Zong, et al., Selective hydrogenolysis of C-O bonds in benzyloxybenzene and dealkaline lignin to valuable aromatics over Ni/TiN, Fuel Process. Technol. 209 (2020) 106523.
[10] N.L. Radhika, S. Sachdeva, M. Kumar, Lignin depolymerization and biotransformation to industrially important chemicals/biofuels, Fuel 312 (2022) 122935.
[11] A.K. Deepa, P.L. Dhepe, Lignin depolymerization into aromatic monomers over solid acid catalysts, ACS Catal. 5 (1) (2015) 365–379.
[12] R. Kumar, V. Strezov, H. Weldekidan, et al., Lignocellulose biomass pyrolysis for bio-oil production: a review of biomass pre-treatment methods for production of drop-in fuel, Renew. Sustain. Energy Rev. 123 (2020) 109763.
[13] D. Carpenter, T.L. Westover, S. Czernik, et al., Biomass feedstocks for renewable fuel production: a review of the impacts of feedstock and pretreatment on the yield and product distribution of fast pyrolysis bio-oils and vapors, Green Chem. 16 (2) (2014) 384–406.
[14] L. Shuai, M.T. Amiri, Y.M. Questell-Santiago, et al., Formaldehyde stabilization facilitates lignin monomer production during biomass depolymerization, Science 354 (6310) (2016) 329–333.
[15] D. Raikwar, K. Van Aelst, T. Vangeel, Elucidating the effect of the physicochemical properties of organosolv lignins on its solubility and reductive catalytic depolymerization, Chem. Eng. J. 461 (2023) 141999.
[16] Z.G. Gong, G.X. Yang, L.L. Huang, et al., Phenol-assisted depolymerisation of condensed lignins to mono-/ poly-phenols and bisphenols, Chem. Eng. J. 455 (2023) 12023.
[17] C.B. Cheng, J. Truong, J.A. Barrett, et al., Hydrogenolysis of organosolv lignin in ethanol/isopropanol media without added transition-metal catalyst, ACS Sustain. Chem. Eng. 8 (2) (2019) 1023–1030.
[18] H. Shafaghat, Y.F. Tsang, J.K. Jeon, et al., In-situ hydrogenation of bio-oil/bio-oil phenolic compounds with secondary alcohols over a synthesized mesoporous Ni/CeO_2 catalyst, Chem. Eng. J. 382 (2020) 122912.
[19] A. Singh, A. Kushwaha, S. Sen, et al., Recent advancement in microwave-assisted pyrolysis for biooil production, Waste-to-Energy Approaches towards Zero Waste (2022) 197–219.
[20] E.C. Gaudino, G. Cravotto, M. Manzoli, et al., From waste biomass to chemicals and energy via microwave-assisted processes, Green Chem. 21 (6) (2019) 1202–1235.
[21] X.D. Liu, F.P. Bouxin, J.J. Fan, et al., Microwave-assisted catalytic depolymerization of lignin from birch sawdust to produce phenolic monomers utilizing a hydrogen-free strategy, J. Hazard. Mater. 402 (2021) 123490.
[22] Z. Shen, C. Shi, F. Liu, et al., Advances in heterogeneous catalysts for lignin hydrogenolysis, Adv. Sci. 11 (1) (2024) 2306693.
[23] Z. Shi, W. Yang, Y. Gu, et al., Metal-nitrogen-doped carbon materials as highly efficient catalysts: progress and rational design, Adv. Sci. 7 (15) (2020) 2001069.
[24] Y. Yang, M. Tan, A. Garcia, et al., Controlling the oxidation state of Fe-based catalysts through nitrogen doping toward the hydrodeoxygenation of m-cresol, ACS Catal. 10 (14) (2020) 7884–7893.
[25] S. Tan, X. Yu, L. Zhu, et al., Heterogeneous iron-catalyzed aerobic oxidative cleavage of C-C bonds in alcohols to esters, ACS Sustain. Chem. Eng. 10 (50) (2022) 16527–16537.
[26] Y. Liu, C. Song, Y. Wang, et al., Rational designed Co@N-doped carbon catalyst for high-efficient H_2S selective oxidation by regulating electronic structures, Chem. Eng. J. 401 (2020) 126038.
[27] Z. Wang, X. Chen, Y. Sun, et al., Co-pyrolysis induced strong metal-support interaction in N-doped carbon supported Ni catalyst for the hydrogenolysis of lignin, Chem. Eng. J. 473 (2023) 145182.
[28] H.B. Yang, S.F. Hung, S. Liu, et al., Atomically dispersed Ni(I) as the active site for electrochemical CO_2 reduction, Nat. Energy 3 (2) (2018) 140–147.
[29] T. Li, H. Lin, X. Ouyang, et al., In situ preparation of Ru@N-doped carbon catalyst for the hydrogenolysis of lignin to produce aromatic monomers, ACS Catal. 9 (7) (2019) 5828–5836.
[30] Y.L. Cao, S.J. Mao, M.M. Li, et al., Metal/porous carbon composites for heterogeneous catalysis: old catalysts with improved performance promoted by N-doping, ACS Catal. 7 (12) (2017) 8090–8112.
[31] C.Y. Su, H. Cheng, W. Li, et al., Atomic modulation of FeCo-nitrogen-carbon bifunctional oxygen electrodes for rechargeable and flexible all-solid-state zinc-air battery, Adv. Energy Mater. 7 (13) (2017) 1602420.
[32] X. Zou, M. Zhai, B. Wang, et al., Molecular-scale elucidating of lignocellulose biomass char steam gasification for ultimately converting to syngas, Fuel Process. Technol. 236 (2022) 107430.
[33] L. Zhang, N. Shang, S. Gao, et al., Atomically dispersed Co catalyst for efficient hydrodeoxygenation of lignin-derived species and hydrogenation of nitroaromatics, ACS Catal. 10 (15) (2020) 8672–8682.
[34] A. Shivhare, D. Jampaiah, S.K. Bhargava, et al., Hydrogenolysis of lignin-derived aromatic ethers over heterogeneous catalysts, ACS Sustain. Chem. Eng. 9 (9) (2021) 3379–3407.
[35] X. Zhang, G.P. Lu, K. Wang, et al., Lignin-derived Zn single atom/N-codoped porous carbon for α-alkylation of aromatic ketones with alcohols via borrowing hydrogen strategy, Nano Res. 15 (3) (2022) 1874–1881.
[36] A. Laobuthee, A. Khankhuean, P. Panith, et al., Ni-Fe cocatalysts on magnesium silicate supports for the depolymerization of kraft lignin, ACS Omega 8 (9) (2023) 8675–8682.
[37] B. Duan, Q. Wang, Y. Zhao, et al., Effect of catalysts on liquefaction of alkali lignin for production of aromatic phenolic monomer, Biomass Bioenergy 131 (2019) 105413.
[38] D. Wang, C. Yuan, C. Yang, et al., Recent advances in catalytic removal volatile organic compounds over metal-organic framework-derived catalysts: a review, Sep. Purif. Technol. (2023) 124765.
[39] B.M. Matsagar, R.X. Yang, S. Dutta, et al., Recent progress in the development of biomass-derived nitrogen-doped porous carbon, J. Mater. Chem. A 9 (7) (2021) 3703–3728.

[40] V. Palma, D. Barba, M. Cortese, et al., Microwaves and heterogeneous catalysis: a review on selected catalytic processes, Catalysts 10 (2) (2020) 246.
[41] Fu. Yishuai, W. Wang, H. Miao, et al., Fabrication of microwave-responsive CMF@CoS_2/MoS_2 catalyst and highly efficient reforming of lignin vapor by microwave irradiation, Acta Chim. Sin. 82 (6) (2024) 596–603.
[42] B. Wang, J. Huang, H. Wu, et al., Synergy of heterogeneous Co/Ni dual atoms enabling selective C-O bond scission of lignin coupling with in-situ N-functionalization, Journal of Energy Chemistry 92 (2024) 16–25.